J. Fluid Mech. (2013), *vol.* 715, *pp.* 359–388.
doi:10.1017/jfm.2012.524

A two-dimensional vortex condensate at high Reynolds number

Basile Gallet† **and William R. Young**

Scripps Institution of Oceanography, La Jolla, CA 92093-0213, USA

(Received 4 August 2012; revised 16 October 2012; accepted 18 October 2012)

We investigate solutions of the two-dimensional Navier–Stokes equation in a $\pi \times \pi$ square box with stress-free boundary conditions. The flow is steadily forced by the addition of a source $\sin nx \sin ny$ to the vorticity equation; attention is restricted to even n so that the forcing has zero integral. Numerical solutions with $n = 2$ and 6 show that at high Reynolds numbers the solution is a domain-scale vortex condensate with a strong projection on the gravest mode, $\sin x \sin y$. The sign of the vortex condensate is selected by a symmetry-breaking instability. We show that the amplitude of the vortex condensate has a finite limit as $\nu \to 0$. Using a quasilinear approximation we make an analytic prediction of the amplitude of the condensate and show that the amplitude is determined by viscous selection of a particular solution from a family of solutions to the forced two-dimensional Euler equation. This theory indicates that the condensate amplitude will depend sensitively on the form of the dissipation, even in the undamped limit. This prediction is verified by considering the addition of a drag term to the Navier–Stokes equation and comparing the quasilinear theory with numerical solution.

Key words: instability, transition to turbulence, vortex flows

1. Introduction

A well-known characteristic of two-dimensional fluid mechanics is the spontaneous emergence of vortices and jets that are significantly larger than the scale of the forcing. In the geophysical and astrophysical context, where the vertical extension of the system is much smaller than the horizontal, these large-scale eddies correspond to global circulations containing a significant part of the total kinetic energy of the flow. Predicting the magnitude of these coherent large-scale structures is a key issue.

Apart from these motivational natural examples, two-dimensional flows have attracted attention because of the simpler form of the equations of motion and the much lighter computational effort required to access the statistically steady state at high Reynolds number. Despite these simplifications, the phenomenology of two-dimensional turbulence is more complex than its three-dimensional counterpart. According to the theories of Kraichnan and Batchelor, the conservation of both energy and enstrophy leads to a forward cascade of enstrophy, from the scale of the forcing to smaller scales, while energy is transferred from the scale of the forcing to larger scales. If energy is steadily injected into a finite-size system, the inverse cascade results in larger and larger eddies, which eventually expand to reach the size of the domain.

† Email address for correspondence: basile.gallet@ens.fr

Then kinetic energy accumulates in a coherent domain-scale vortex, which, according to Kraichnan (1967), is analogous to Bose–Einstein condensation.

Numerical and experimental studies aimed at studying the statistically steady state of forced and dissipative two-dimensional turbulence have used several different types of forcing. Most popular in numerical studies is white-in-time random forcing acting on a narrow band of wavenumbers (Lilly 1969; Maltrud & Vallis 1991; Smith & Yakhot 1994; Boffetta 2007; Chertkov *et al.* 2007). White-noise forcing has the property that the rate at which energy is injected into the flow is a control parameter, i.e. watts per kilogram delivered to the fluid by the forcing is constant no matter how energetic the flow becomes. Thus at first the amplitude of the condensate increases as the square root of time (Chertkov *et al.* 2007; Chertkov, Kolokolov & Lebedev 2010). At times of order ν^{-1} (ν is the small viscosity) saturation is achieved when viscous damping of the gravest mode is significant, which requires that large-scale velocities are of order $\nu^{-1/2}$. To avoid this runaway and achieve a statistically steady state with subsonic velocities, one must prevent accumulation of energy on scales comparable to the domain by adding 'large-scale dissipation' to the problem. Unfortunately, important characteristics of the statistically steady flow are strongly sensitive to how this large-scale damping is implemented (Tsang 2010).

On the other hand, in some experimental studies the fluid is driven via the Lorentz force, which is equivalent to prescribing a body force (Sommeria 1986; Paret & Tabeling 1997; Paret, Jullien & Tabeling 1999). The forcing is either steady or varies on a time scale of a few seconds. In this circumstance the rate of working of the force (the product of force and fluid velocity) is not fixed *a priori*. If the large-scale flow becomes more energetic, then advection by large eddies disrupts the phase relation between the force and forcing-scale eddies and thus reduces the energy injection rate (Tsang & Young 2009). This phase disruption is a crucial difference between steady forcing and white-noise forcing. We show here that phase disruption saturates the energy input so that large-scale dissipation is not required to achieve a statistically steady flow. Moreover, the amplitude of the saturated condensate is independent of ν.

We use analytic and numerical techniques to study the large-scale condensate of a two-dimensional flow inside a square domain (a box) driven by a steady body force. We focus on the case in which the only damping is via Navier–Stokes viscosity. The planform of the forcing is a single Helmholtz eigenmode of the box. Previous studies of these 'Kolmogorov flows' have focused on weakly nonlinear regimes close to the threshold of instability of the viscous laminar solution (Meshalkin & Sinai 1961; Thess 1992; Gama, Vergassola & Frisch 1994), where amplitude equations can be obtained for the large-scale flow (Sivashinsky 1985). By contrast, our study extends to the strongly nonlinear regime corresponding to very low values of ν. In this latter regime, the condensate dominates the flow, and expansion around the condensate opens an analytic avenue. In particular, we compute the amplitude of the condensate, and show that this amplitude is independent of viscosity in the inviscid limit. This high-Reynolds-number scaling regime might give the incorrect impression that viscosity is unimportant. However, the realized solution is determined via viscous selection of a preferred solution from a family of solutions to the inviscid problem (the forced Euler equation). In this sense, viscosity is vital.

In § 2 we introduce the system and provide numerical evidence for condensation: at low viscosity the system settles in a time-independent state with a large-scale condensate. In § 3 we introduce the quasilinear approximation, under which we provide an analytical description of these steady solutions. We compute a continuous family of solutions to the inviscid problem and consideration of infinitesimal ν

then provides a selection criterion that determines the amplitude of the condensate. Section 4 is a boundary-layer analysis. Solving for the boundary layers that develop on the sidewalls of the square domain extends the analytical results to small but finite viscosity. Section 5 compares the analytic predictions of the condensate amplitude with numerical solution. We discuss the selection mechanism in greater details in § 6. Although the amplitude of the condensate is selected by viscosity, the amplitude is independent of ν. Using symmetry considerations, we show that this selection mechanism is relevant to a class of weakly damped triadic systems in which an unstable degree of freedom is driven by a steady external force. We consider an elementary mechanical system that illustrates the key features of the selection mechanism without the involved algebra of the fluid problem. The selected solution is independent of the damping coefficient but strongly dependent on the form of the damping term. To illustrate this point, we consider in § 7 bottom drag and hyperviscosity in the Navier–Stokes equation. Section 8 is the conclusion, and technical details are contained in three appendices.

2. Forced Kolmogorov flows in a square domain

We consider the two-dimensional motion of a fluid in a square box. We non-dimensionalize the length so that the domain is $(x, y) \in [0, \pi]^2$. The streamfunction is denoted as $\psi(x, y, t)$, and vorticity is $-\Delta\psi$, where $\Delta = \partial_x^2 + \partial_y^2$ is the Laplacian. The two-dimensional Navier–Stokes equation is then

$$\Delta\psi_t + J(\Delta\psi, \psi) = \sin nx \sin ny + \nu\Delta^2\psi, \tag{2.1}$$

where $J(a, b) = a_x b_y - a_y b_x$ is the Jacobian and ν is the inverse of the Reynolds number. The first term on the right of (2.1) is the curl of a body force, which drives $n \times n$ counter-rotating vortices with n an even integer. We restrict attention to even n so that the forcing does not apply a net torque on the fluid, i.e. the integral of the forcing over the domain is zero. In the following we focus on the cases $n = 2$ and $n = 6$, although similar results apply to arbitrary even n. In fact, $n = 2$ is the simplest example, and $n = 6$ was the electromagnetic forcing protocol used by Sommeria (1986) in an experimental study.

We use no-penetration, stress-free boundary conditions, so that the streamfunction ψ and the vorticity $-\Delta\psi$ vanish on the boundary. The streamfunction is thus efficiently projected onto the basis $\sin px \sin qy$, where p and q are positive integers. We use a standard pseudo-spectral method to solve (2.1).

At high values of viscosity, the laminar solution

$$\psi_L = -\frac{\sin nx \sin ny}{4\nu n^4} \tag{2.2}$$

is stable; provided the viscosity is large enough, ψ_L is an attractor (see figure 1). For lower values of ν, the laminar solution ψ_L is unstable, and then a global circulation with a single vortex filling the domain is observed; see figure 2.

With even n, the sense of rotation of the global circulation is an accident of initial conditions, i.e. there is a symmetry-breaking instability. Following Kraichnan (1967), the spontaneous formation of a single large-scale vortex is known as 'condensation'. Condensation is usually regarded as the end-point of a turbulent inverse cascade of energy. However, in figure 2 the flow is steady. Indeed, although there are small-scale structures in the vorticity field, the global circulation is a steady and stable solution

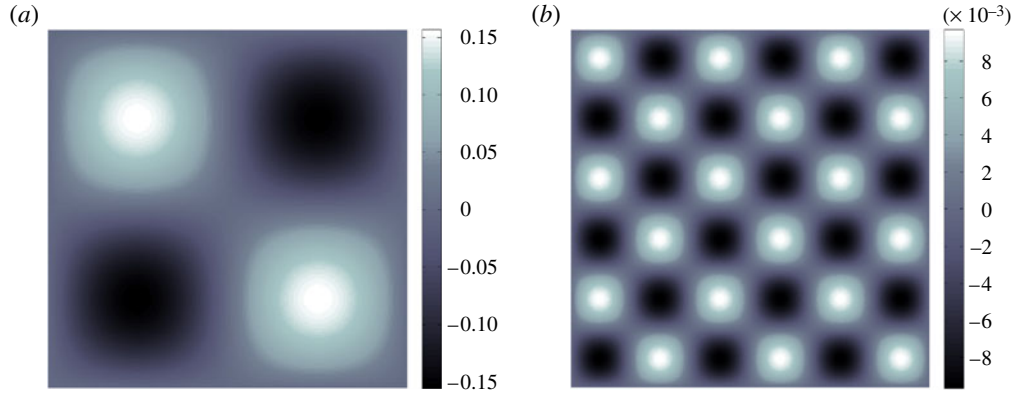

FIGURE 1. (Colour online) Streamfunction attained after the transient, in numerical solutions with relatively large viscosity: (*a*) $n = 2$ and $\nu^{-1} = 10$; (*b*) $n = 6$ and $\nu^{-1} = 50$. At these values of ν, the laminar solution in (2.2) is stable.

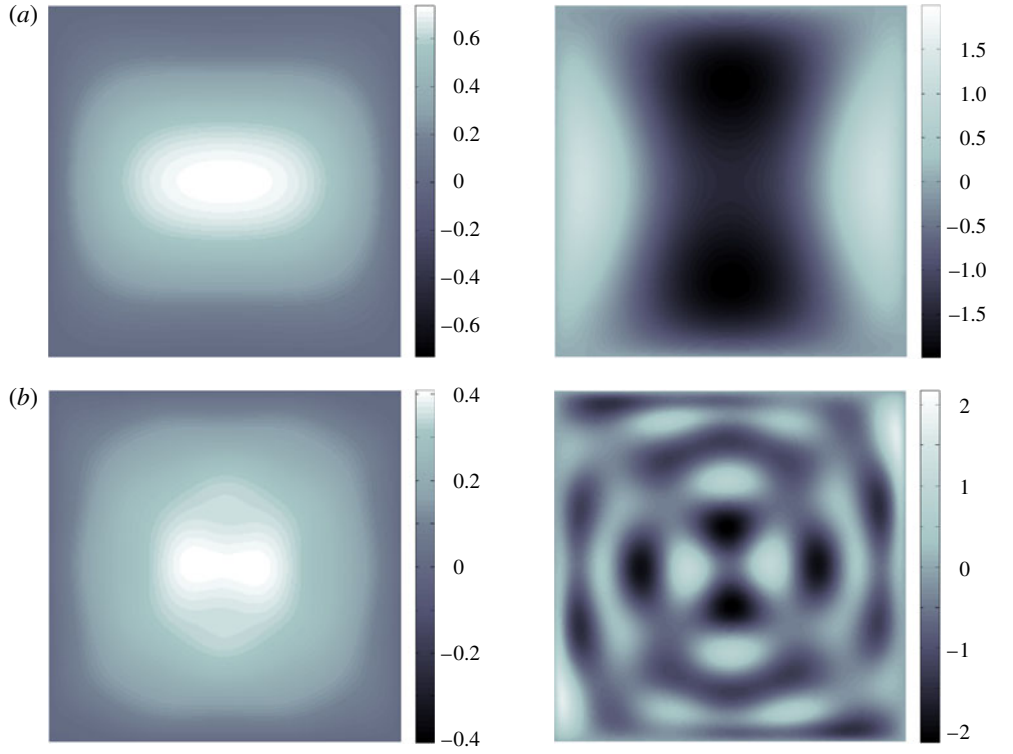

FIGURE 2. (Colour online) Snapshots of the stationary solution reached at large times in a direct numerical solution of (2.1): (*a*) $n = 2$ and $\nu^{-1} = 2000$; (*b*) $n = 6$ and $\nu^{-1} = 1000$. The panels on the left show the streamfunction, which is dominated by a large-scale condensate; those on the right show the vorticity. The latter exhibit structures of typical size n^{-1} that coexist with the condensate.

of (2.1) even for very low values of viscosity (a few times 10^{-5} for $n = 2$, and 10^{-3} for $n = 6$). We discuss the transition to time dependence further in § 5.

As ν decreases, the amplitude of the condensate increases and saturates to a ν-independent asymptotic value. The goal of the present study is to understand in mechanistic detail how energy is transferred from the $n \times n$ forcing in (2.1) to the vortex condensate, and to determine the amplitude of the condensate as a function of the parameter ν, with an emphasis on the limit $\nu \to 0$.

3. Quasi-linear approximation

As anticipated by the Kraichnan–Batchelor theory, there is strong accumulation of energy in the gravest mode,

$$\chi(x, y) \stackrel{def}{=} \sin x \sin y, \tag{3.1}$$

when ν is small. The streamfunction is then dominated by the grave mode χ, and substantial analytic progress is made by assuming that ψ can be expanded around this solution of the Euler equation. We thus write

$$\psi(x, y, t) = a(t)\chi(x, y) + \phi(x, y, t), \tag{3.2}$$

where a is the amplitude of the condensate and, by definition, ϕ has no projection on the gravest mode χ. The condition of no projection is

$$\langle \phi\chi \rangle = 0, \tag{3.3}$$

where $\langle\ \rangle$ denotes the average over the box. The field ϕ will be referred to as the 'remainder', or the 'small-scale remainder', although the latter denomination is strictly justified only for large n.

Inserting the decomposition equation (3.2) into the Navier–Stokes equation (2.1), using $\Delta\chi = -2\chi$ and the no-projection condition (3.3) leads to

$$\Delta\phi_t + J(\Delta\phi + 2\phi, a\chi) + \mathscr{N} = \sin nx \sin ny + \nu\Delta^2\phi, \tag{3.4}$$

$$\tfrac{1}{2}a_t = \langle J(\Delta\phi, \phi)\chi \rangle - \nu a. \tag{3.5}$$

In (3.4) the nonlinear term corresponding to self-interaction of the small-scale remainder is

$$\mathscr{N} \stackrel{def}{=} J(\Delta\phi, \phi) - 4\chi\langle J(\Delta\phi, \phi)\chi \rangle. \tag{3.6}$$

Notice that the remainder equation (3.4) has no projection on the grave mode χ.

The quasilinear (QL) approximation consists in discarding the nonlinear term $\mathscr{N}$ in (3.4). The motivation for the QL approximation is that, if there is strong condensation into the grave mode χ, then in (3.4) $J(\Delta\phi, a\chi) \gg \mathscr{N}$. We make the QL approximation, $\mathscr{N} \to 0$, and assess its validity via comparison with numerical solutions of the full system.

3.1. *A family of solutions in the inviscid limit*

Let us consider the QL problem with very weak viscosity, $\nu \ll 1$. In the interior of the domain we can seek a solution of the form

$$\phi = \phi_0 + \nu\phi_1 + \nu^2\phi_2 + \cdots. \tag{3.7}$$

We write

$$q(x, y) \stackrel{def}{=} \Delta\phi_0 + 2\phi_0, \tag{3.8}$$

so that at leading order the QL version of (3.4) is

$$a(q_x \sin x \cos y - q_y \cos x \sin y) = \sin nx \sin ny. \tag{3.9}$$

One can divide this equation by $\cos x \cos y$ and make use of the change of variables $X = \ln(\sin x)$ and $Y = \ln(\sin y)$ to get

$$q_X - q_Y = \frac{\sin nx \sin ny}{a \cos x \cos y} = \frac{1}{a} U_{n-1}(\mathrm{e}^X) U_{n-1}(\mathrm{e}^Y), \tag{3.10}$$

where U_{n-1} is the Chebyshev polynomial of the second kind of order $n-1$. Upon developing the product on the right-hand side of this equation for a given n, one gets a sum of exponentials in X and Y, each of which can be easily integrated. For instance, for $n = 2$ the right-hand side product is $\mathrm{e}^{X+Y} 4/a$, which by integration yields $[2(X-Y)/a]\mathrm{e}^{X+Y}$.

Thus, with $n = 2$, the solution of (3.9) is

$$q = \frac{2}{a} \chi \ln\left(\frac{\sin x}{\sin y}\right). \tag{3.11}$$

With $n = 6$, the solution of (3.9) is

$$q = \frac{12}{a}\left[\ln\left(\frac{\sin x}{\sin y}\right)(9\chi + 256\chi^3 + 256\chi^5) + (\sin^2 y - \sin^2 x)(48\chi + 256\chi^3) + 24\chi(\sin^4 x - \sin^4 y)\right]. \tag{3.12}$$

One can add a homogeneous solution, $f(\chi)$, with f an arbitrary function, to (3.11) and (3.12). However, we determine that $f(\chi) = 0$ using symmetry considerations described in figure 9: under a rotation of angle $\pi/2$ around the centre of the square domain (denoted as $\mathscr{R}$ in figure 9), the forcing term changes sign, but χ does not. According to (3.4), we thus expect ϕ_0 to change sign under this transformation. Hence q must change sign under the transformation $(x, y) \to (\pi - y, x)$, which implies $f(\chi) = 0$. This conclusion, that $f(\chi) = 0$, is also reached using the Prandtl–Batchelor theorem as a solvability condition at next order in ν.

The streamfunction and vorticity fields of the leading-order remainder ϕ_0 can be obtained from the expressions in (3.11) and (3.12) by inverting $q = \Delta\phi_0 + 2\phi_0$. The solution can be accomplished either numerically or analytically using a Fourier series (see appendix A). The vorticity $-\Delta\phi_0$ of the remainder is presented in figure 3. A comparison with figure 2 shows that the QL remainder vorticity, $-a\Delta\phi_0$, captures the main structures of the total vorticity field, $-\Delta\psi$, of the full nonlinear problem.

The symmetry considerations outlined above also show that

$$\langle \chi J(\Delta\phi_0, \phi_0) \rangle = 0. \tag{3.13}$$

Thus the steady version of the amplitude equation (3.5) is satisfied at leading order by any value of amplitude a.

Note, too, that the rate of working of the force in (2.1) is

$$\varepsilon \stackrel{def}{=} -\langle \psi \sin nx \sin ny \rangle, \tag{3.14}$$

and symmetry also shows that $\langle (a\chi + \phi_0) \sin nx \sin ny \rangle = 0$. That is, the inviscid solution in (3.11) and (3.12) is not extracting energy (nor enstrophy) from the applied $n \times n$ force.

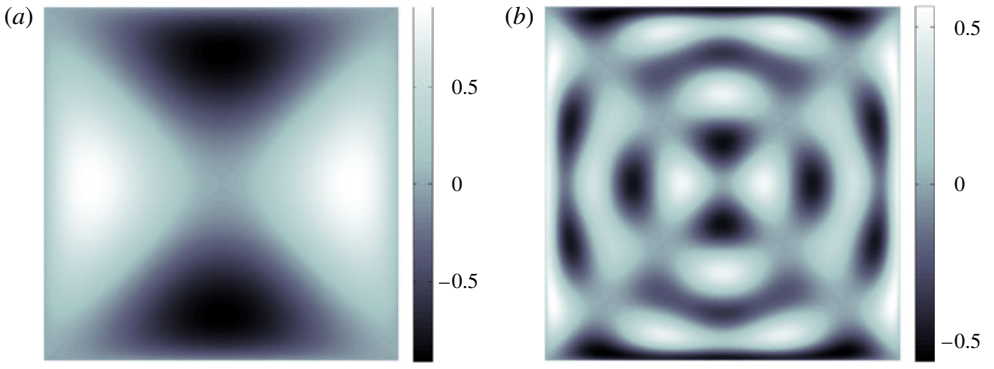

FIGURE 3. (Colour online) The inviscid solution for the vorticity of the remainder in the QL approximation. We plot $-a\Delta\phi_0$ for (*a*) $n = 2$ and (*b*) $n = 6$. One observes the same small-scale vorticity structures as in figure 2, without the large-scale vorticity of the condensate.

To summarize, we have obtained a continuous family of solutions to the forced, inviscid QL problem. The streamfunction in (3.2) consists of a condensate of amplitude a together with a remainder of amplitude $1/a$. Any value of a is acceptable at this stage, and, provided a is large enough for the QL approximation to be valid, this solution is a good approximation to a solution of the full nonlinear forced inviscid equation.

3.2. *Selection by viscosity of a ν-independent solution*

Viscosity is required to select one solution from the continuous family of solutions parametrized by a. A straightforward approach is to consider the $O(\nu)$ terms from the remainder equation (3.4), and solve to obtain ϕ_1. The average Jacobians $\langle\chi J(\Delta\phi_0, \phi_1)\rangle$ and $\langle\chi J(\Delta\phi_0, \phi_1)\rangle$ are non-zero, and thus the amplitude equation (3.5) determines a at order $O(\nu)$.

To avoid the direct assault outlined above, we consider the energy and enstrophy budgets obtained by multiplying the stationary version of (2.1) respectively with ψ and $\Delta\psi$:

$$0 = \langle\psi \sin nx \sin ny\rangle + \nu\langle(\Delta\psi)^2\rangle, \tag{3.15}$$

$$0 = \langle\Delta\psi \sin nx \sin ny\rangle + \nu\langle\Delta^2\psi\,\Delta\psi\rangle. \tag{3.16}$$

Integrating by parts the first term on the right of (3.16) gives $-2n^2\langle\psi \sin nx \sin ny\rangle$, which can be expressed using (3.15) to give

$$2n^2\langle(\Delta\psi)^2\rangle = \langle|\boldsymbol{\nabla}\Delta\psi|^2\rangle. \tag{3.17}$$

This crucial relation traces back to the harmonic forcing having production rates of enstrophy and energy in a ratio $2n^2$. Therefore any acceptable solution of the problem must have the same ratio $2n^2$ between its rates of dissipation of enstrophy and energy. Inserting $\psi = a\chi + \phi$ into (3.17) gives the amplitude of the global circulation as

$$a = \pm\sqrt{\frac{\langle|\boldsymbol{\nabla}\Delta\phi|^2\rangle - 2n^2\langle(\Delta\phi)^2\rangle}{2(n^2-1)}}. \tag{3.18}$$

The averages on the right of (3.18), and thus the value of a, are computed using ϕ_0 in appendix A for $n = 2$. For $n = 6$, these averages are computed numerically from (3.12).

The analytic result for $n = 2$ is

$$|a| = 2^{-3/4}3^{-1/2}\left(75 - 4\pi^2 - \frac{\pi^4}{5}\right)^{1/4} \simeq 0.687, \tag{3.19}$$

and for $n = 6$ is

$$|a| \simeq 0.682. \tag{3.20}$$

These results are compared with numerical results for the full nonlinear systems in § 5; a in (3.19) is within 10 % of the full nonlinear value, and a in (3.20) is within 30 % of the full nonlinear value. Although the error in the case with $n = 6$ is rather large, the QL approximation gives accurate predictions for the velocity near the periphery of the domain where the velocity associated with χ is large.

We emphasize that the amplitude of the condensate is selected by the viscous term of the Navier–Stokes equation even though a has a finite limit, given by (3.19) and (3.20), as $\nu \to 0$. A detailed discussion of this selection mechanism is given in § 6. This section also presents a much simpler system exhibiting the same selection mechanism: a spinning solid driven by a constant torque in the limit of weak damping. The reader desiring more insight into the selection mechanism can move directly to § 6.

4. Viscous solution and boundary layers

In (3.19) and (3.20) the amplitude a is computed using the inviscid solution ϕ_0. However, the expressions (3.11) and (3.12) indicate that the leading-order vorticity is

$$-\Delta\phi_0 \propto y \ln y \quad \text{as } y \to 0. \tag{4.1}$$

(There are analogous expressions for $\Delta\phi_0$ at the other three walls.) Although the leading-order vorticity $\Delta\phi_0$ vanishes at the boundary, the derivatives are singular, and

$$\Delta^2\phi_0 \propto y^{-1} \quad \text{as } y \to 0. \tag{4.2}$$

In fact, evaluating (3.4) on the boundary shows that $\Delta^2\phi = 0$ is the correct boundary condition. The singularity in $\Delta^2\phi_0$ indicates that there are viscous boundary layers at the walls.

This divergence in (4.2) originates because the velocity field associated with χ has stagnation points in each of the four corners. At leading order, the inviscid QL problem (3.9) is a balance between advection by χ and the forcing $\sin nx \sin ny$; a fluid element passing close to a corner moves slowly and accumulates a lot of vorticity from the forcing in this region.

To heal the boundary singularity in (4.2), it is necessary to include the viscous term at leading order, e.g. with a boundary-layer analysis. The solution of this boundary-layer problem is well behaved at the boundaries of the square domain and provides the viscous corrections to the inviscid results in (3.19) and (3.20). This boundary-layer analysis amounts to solving an advection–diffusion problem with sources and sinks in the high-Péclet-number limit.

4.1. *Inner solution*

We focus on $n = 2$, which is simpler from a mathematical point of view but easy to generalize to arbitrary even n. For small viscosity, the viscous term can be neglected in the bulk of the domain (the outer region) to arrive at the outer solution for q in (3.11). This approximation fails close to the boundaries, where there are boundary layers. One

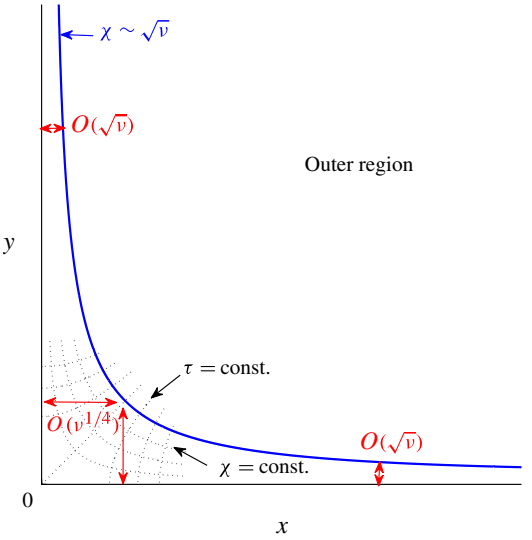

FIGURE 4. (Colour online) In the vicinity of a corner, a streamline of constant $\chi \sim \sqrt{\nu}$ connects a wall inner region of width $O(\sqrt{\nu})$ to a corner patch of spatial extension $O(\nu^{1/4})$.

must distinguish between the *wall regions*, where there is fast variation with respect to the coordinate perpendicular to the wall, and the *corner regions*, where there is fast variation with respect to both coordinates. Indeed, close to a wall, say the southern wall at $y = 0$, the viscous term must be taken into account in a boundary layer of thickness $y = O(\sqrt{\nu})$, with $x = O(1)$. The corresponding streamlines have $\chi = O(\sqrt{\nu})$. As we follow such a streamline into the neighbourhood of the corner $(0, 0)$, x and y become of the same order of magnitude, so that $x \sim y \sim \sqrt{\chi} \sim \nu^{1/4}$ (see e.g. Childress 1979). Thus the wall boundary layer is thinner than the corner 'patch'. The wall boundary layer and the corner patch are sketched in figure 4. These considerations motivate the following asymptotic analysis.

The remainder ϕ varies rapidly inside the boundary layers, hence $\Delta\phi \gg \phi$ and $\Delta q \simeq \Delta^2\phi$. The QL equation for the inner problem thus reduces to an advection–diffusion equation for the inner solution $q^{(i)}$:

$$aJ(q^{(i)}, \chi) = \sin 2x \sin 2y + \nu \Delta q^{(i)}. \tag{4.3}$$

A standard technique to solve this boundary-layer problem close to a wall is the von Mises transformation, which turns the advection–diffusion problem into a heat equation. Furthermore, close to a corner, conformal mapping can be used to map the corner region into a half-plane. The flow becomes uniform and parallel after the conformal transformation, so that the advection–diffusion problem is again turned into a heat equation. In the following, we make use of a convenient change of coordinates, which reduces to the von Mises variables close to a wall, and to the conformal mapping variables close to a corner. This conveniently unifies the analysis of the corner patches and the wall layers, resulting in a heat equation, with a source term arising from the $\sin 2x \sin 2y$ forcing.

Thus let us consider $a > 0$ and introduce the function

$$\tau \stackrel{def}{=} \cos y - \cos x. \tag{4.4}$$

We change coordinates from (x, y) to (τ, χ): τ describes variations of $q^{(i)}$ along the peripheral streamlines, while χ tracks variations of $q^{(i)}$ across the streamlines. Rosenbluth *et al.* (1987) used a similar coordinate transform to solve the problem of advection–diffusion of a tracer by a cellular flow at high Péclet number. The present analysis differs from that of Rosenbluth *et al.* by the presence of a source term in (4.3). Denoting by $\mathscr{J}$ the Jacobian of the change of variables, the three terms in (4.3) are

$$J(q^{(i)}, \chi) = \mathscr{J} q_\tau, \tag{4.5}$$

$$\sin(2x)\sin(2y) = 4\chi(1 - \sqrt{\chi^2 + \tau^2}) \tag{4.6}$$

and

$$\begin{aligned}\Delta q^{(i)} = &-\tau q_\tau - 2\chi q_\chi - 2\chi\tau q_{\tau\chi} + (2\sqrt{\chi^2+\tau^2} - \tau^2) q_{\tau\tau} \\ &+ (2\sqrt{\chi^2+\tau^2} - \tau^2 - 2\chi^2) q_{\chi\chi}.\end{aligned} \tag{4.7}$$

A drawback of this change of variables is that there are two points in the square domain that correspond to a single value of (τ, χ). These two points are symmetric with respect to the diagonal $y = \pi - x$ of the square. We thus focus on the southwest half of the square, $y < \pi - x$, where the value of the Jacobian is

$$\mathscr{J} = \sqrt{(\chi^2 + \tau^2)[\tau^2 + 4(1 - \sqrt{\chi^2 + \tau^2})]}. \tag{4.8}$$

The solution in the northeast half of the square is obtained via symmetry.

All the expressions above simplify very considerably in the peripheral region, where $\chi \ll 1$.

4.2. *The wall boundary layer*

Close to a wall and away from the corners, the inner solution varies rapidly across the streamlines, and slowly along the streamlines. We thus introduce an inner variable $\chi = \sqrt{\nu}\tilde{\chi}$, with $\tilde{\chi} = O(1)$ and $\tau = O(1)$, and scale the inner solution as $q^{(i)} = \sqrt{\nu}\tilde{q}$. It proves efficient to solve (4.3) for the viscous term $\Delta q^{(i)}$ instead of $q^{(i)}$. To lowest order in ν this field is

$$\Delta q^{(i)} = q^{(i)}_{\chi\chi}(\sin^2 x + \sin^2 y), \tag{4.9}$$

with $\sin^2 y \gg \sin^2 x$ close to the eastern and western walls, while $\sin^2 x \gg \sin^2 y$ close to the northern and southern walls. We thus introduce $s \overset{def}{=} q^{(i)}_{\chi\chi}$ and look for the solution for s. The scaling $s = \tilde{s}/\sqrt{\nu}$ follows from the scalings for $q^{(i)}$ and χ, i.e. $\tilde{s} = \tilde{q}_{\tilde{\chi}\tilde{\chi}}$. Keeping the leading order only in expressions (4.5)–(4.7) leads to

$$\tilde{q}_\tau = 4\tilde{\chi}\frac{1 - |\tau|}{2|\tau| - \tau^2} + \tilde{q}_{\tilde{\chi}\tilde{\chi}}. \tag{4.10}$$

We get rid of the source term in this heat equation by differentiating twice with respect to $\tilde{\chi}$. This leads to the homogeneous heat equation

$$a\tilde{s}_\tau = \tilde{s}_{\tilde{\chi}\tilde{\chi}}. \tag{4.11}$$

Solving for the field $\Delta q^{(i)}$ (instead of $q^{(i)}$) amounts to solving a homogeneous heat equation close to the walls, instead of an inhomogeneous one. The main balance in (4.11) is thus between advection and diffusion, the forcing being negligible.

4.3. *The corner patches*

Close to the corners, where $\tau \ll 1$, the denominator of the source term in (4.10) becomes small and the wall approximation breaks down. In these regions the inner solution evolves rapidly with respect to both τ and χ. We focus on the corner at $(x, y) = (0, 0)$ (the southwest corner), and introduce the corner region scalings through the inner variables $\chi = \sqrt{\nu}\tilde{\chi}$ and $\tau = \sqrt{\nu}\tilde{\tau}$. Keeping the leading order in expressions (4.5)–(4.7) leads to

$$a\tilde{q}_{\tilde{\tau}} = \frac{2\tilde{\chi}}{\sqrt{\tilde{\tau}^2 + \tilde{\chi}^2}}. \tag{4.12}$$

The main balance in the corners is between advection and forcing, while the viscous term is negligible. Similar equations can be constructed at the other three corners. Note particularly that, because n is even, the sign of the source on the right-hand side of (4.12) is reversed at the southeast and northwest corners.

Because the integral from $\tau = -\infty$ to $\tau = +\infty$ of the source on the right of (4.12) is divergent, it is once again easier to deal with the field $\tilde{s} = \tilde{q}_{\tilde{\chi}\tilde{\chi}}$. Differentiating (4.12) twice with respect to $\tilde{\chi}$ yields

$$a\tilde{s}_{\tilde{\tau}} = -\frac{6\tilde{\tau}^2\tilde{\chi}}{(\tilde{\tau}^2 + \tilde{\chi}^2)^{5/2}}. \tag{4.13}$$

We can now integrate (4.13) around the corner, that is, from $\tilde{\tau} = -\infty$ to $\tilde{\tau} = +\infty$ at constant $\tilde{\chi}$, to get a finite corner-turning jump:

$$a(\tilde{s}|_{(\tilde{\tau}=+\infty,\tilde{\chi})} - \tilde{s}|_{(\tilde{\tau}=-\infty,\tilde{\chi})}) = -\int_{-\infty}^{\infty} \frac{6\tilde{\tau}^2\tilde{\chi}}{(\tilde{\tau}^2 + \tilde{\chi}^2)^{5/2}}\,\mathrm{d}\tilde{\tau} = -\frac{4}{\tilde{\chi}}. \tag{4.14}$$

Thus each corner injects a non-integrable singularity, $\pm 4/\tilde{\chi}$, into the field s. These singular injections alternate in sign, and are smoothed by diffusive evolution along the wall boundary layers, and the boundary condition $\phi = q = s = 0$ at $\tilde{\chi} = 0$.

4.4. *A periodically forced heat equation*

Now we construct the full peripheral solution for $s(\tau, \chi)$ by 'unwrapping' the boundary layer and considering the time-like variable τ in (4.11) to run from $-\infty$ to ∞. The corner singularities are injected whenever the flow turns a corner with singular structure $-4/\chi$ at $\tau = 0, \pm 4, \pm 8, \ldots$, and with $+4/\chi$ at $\tau = \pm 2, \pm 6, \pm 10, \ldots$. This periodic-in-$\tau$ version of the problem enforces the correct boundary conditions on s. The restriction of the solution to the interval $\tau \in [0, 2]$ is the boundary-layer solution close to the southern wall. Thus the peripheral distribution is determined by solving the periodically forced diffusion equation:

$$as_\tau = -\frac{4}{\chi}\sum_{p=-\infty}^{\infty}(-1)^p\,\delta(\tau - 2p) + \nu s_{\chi\chi}. \tag{4.15}$$

Considering only the $p = 0$ term in the series in (4.15), we have the forced diffusion equation

$$af_\tau = -\frac{4}{\chi}\delta(\tau) + \nu f_{\chi\chi}, \tag{4.16}$$

with a similarity solution

$$f(\tau,\chi) = -\frac{4}{\sqrt{a\nu\tau}}\mathscr{D}\left(\frac{\chi}{2}\sqrt{\frac{a}{\nu\tau}}\right)H(\tau). \tag{4.17}$$

Above, $H(\tau)$ is the step function, and

$$\mathscr{D}(x) = \mathrm{e}^{-x^2}\int_0^x \mathrm{e}^{t^2}\,\mathrm{d}t \tag{4.18}$$

is Dawson's integral. The solution (4.17) shows how the χ^{-1} initial singularity in (4.16) is healed by diffusion. The solution to (4.15) can now be expressed as an infinite sum of these Dawson similarity solutions. In particular, near the wall at $y = 0$, this solution is

$$s(\tau,\chi) = 4\sum_{p=0}^{\infty}\frac{(-1)^{p+1}}{\sqrt{a\nu(\tau+2p)}}\mathscr{D}\left(\frac{\chi}{2\sqrt{(\nu/a)(\tau+2p)}}\right). \tag{4.19}$$

4.5. *Matching*

From this expression for s, the diffusive term $\Delta q^{(i)} \simeq s(\tau,\chi)\sin^2 x$ is obtained for the inner solution close to $y = 0$. In the QL approximation, Δq is odd under a rotation of $\pi/2$ around the centre of the square (see figure 9), and this rotation can be used to get the boundary layers near the other walls. One obtains the following final expression for $\Delta q^{(i)}$, which includes the four boundary layers:

$$\begin{aligned}\Delta q^{(i)} &= \sin^2 x\; s(1-\cos x\cos y, \sin x\sin y) - \sin^2 y\; s(1+\cos x\cos y, \sin x\sin y)\\ &= \sin^2 y\sum_{p=0}^{\infty}\frac{4\,(-1)^p}{\sqrt{a\nu(\cos x\cos y+2p+1)}}\mathscr{D}\left(\frac{\sin x\sin y}{2\sqrt{(\nu/a)(\cos x\cos y+2p+1)}}\right)\\ &\quad -\sin^2 x\sum_{p=0}^{\infty}\frac{4\,(-1)^p}{\sqrt{a\nu(-\cos x\cos y+2p+1)}}\mathscr{D}\left(\frac{\sin x\sin y}{2\sqrt{(\nu/a)(-\cos x\cos y+2p+1)}}\right).\end{aligned} \tag{4.20}$$

Although the series expression for s converges slowly, its asymptotic behaviour for small and large χ can be computed using Mellin's transform, as described in appendix B: it behaves as χ for $\chi \ll \sqrt{\nu}$, and as χ^{-1} for $\chi \gg \sqrt{\nu}$. The corresponding $\Delta q^{(i)}$ is thus compatible with the boundary conditions at $\chi = 0$, where it must vanish, and it matches the divergence of the outer solution for Δq at large $\chi/\sqrt{\nu}$.

In order to achieve the matching of Δq, we add to (4.20) all the terms in the Laplacian of the outer solution (3.11) that do not diverge at the boundaries. This final expression for Δq can then be inverted numerically in Fourier space to get q, the vorticity and the streamfunction of the stationary solution. Note that the procedure is exactly the same for arbitrary even n: the y^{-1} divergence of the outer solution for Δq always originates from a term of the form $\sin x\sin y\ln(\sin x/\sin y)$ in q. Up to a prefactor, the same boundary-layer solution for s can be obtained, and the same matching procedure can be used to get the total Δq.

We compare in figure 5 the viscous term $\Delta^2\psi$ obtained from the boundary-layer analysis to numerical solutions of the QL and full nonlinear (NL) systems: the inner solution reproduces very accurately the boundary layers of the QL solution. These boundary layers resemble those of the NL system. There is one main difference: a rotation by angle $\pi/2$ around the centre of the square together with a sign change

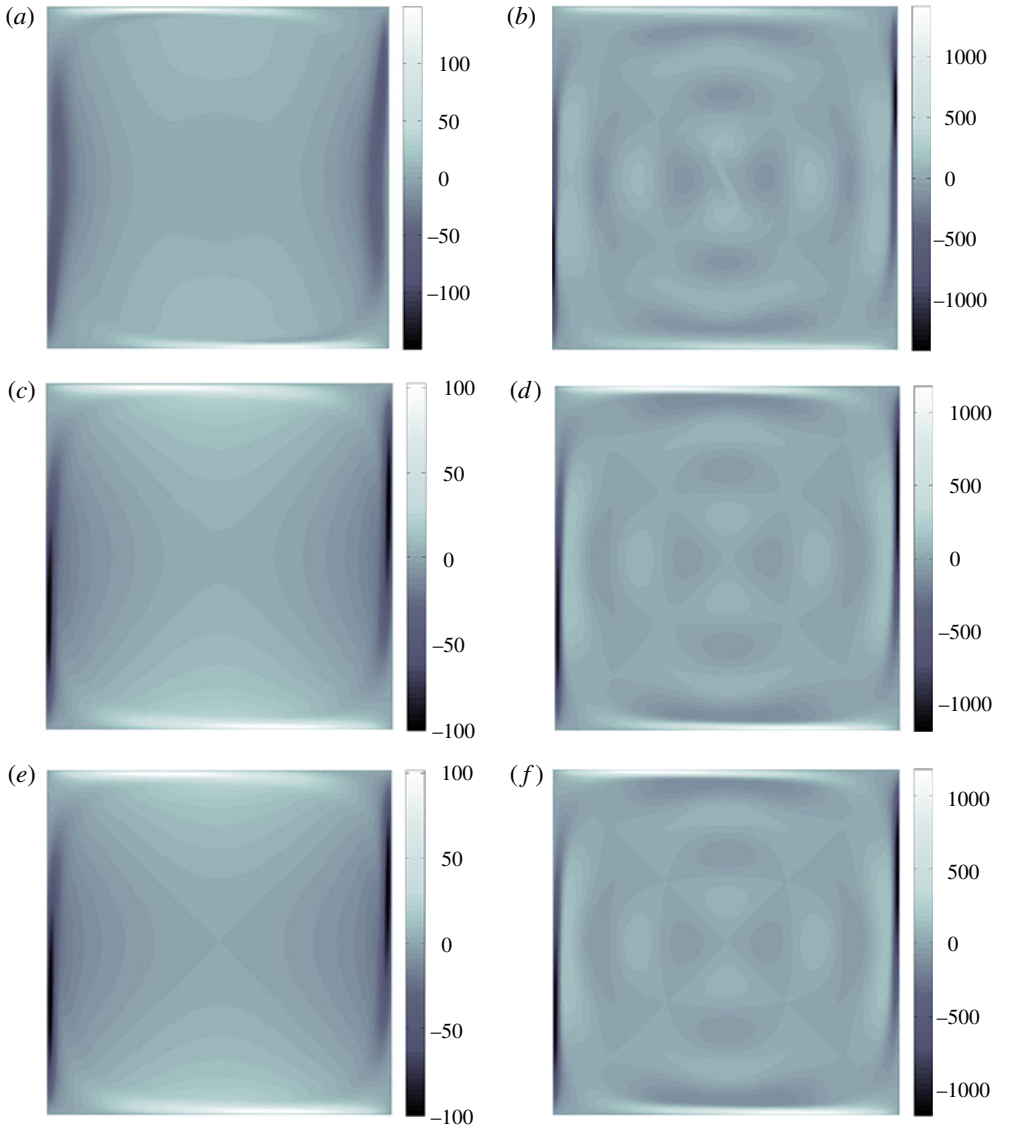

FIGURE 5. (Colour online) The viscous term $\Delta^2\psi$ from the numerical solution of the full nonlinear (NL) system (*a*,*b*) is compared to $\Delta^2\psi$ from a numerical solution of the quasilinear (QL) system of equations (*c*,*d*) and to that from the solution of the boundary-layer analysis (*e*,*f*). Left-hand panels (*a*,*c*,*e*) $n = 2$ and $\nu^{-1} = 2000$; right-hand panels (*b*,*d*,*f*) $n = 6$ and $\nu^{-1} = 4000$. The inner solution reproduces very accurately the boundary layers of the QL solution. These boundary layers resemble those of the NL solution. However, there is a slight advection of these latter by the small-scale velocity, which cannot be described by the QL approximation.

of ϕ is a symmetry of the QL system, but not of the NL system. Therefore, the boundary layers close to walls in x and y are not identical up to a change in sign of the NL solution. The NL system includes advection of these boundary layers by the small-scale flow: for $n = 2$ and positive a, this small-scale flow pulls the boundary

layers in x away from the walls and pushes the boundary layers in y against the walls, as can be seen in figure 5(a).

5. Amplitude of the condensate

The amplitude a of the condensate in the boundary-layer approximation is given by (3.18) and we can now evaluate the right-hand side using a ϕ that is improved by the viscous boundary-layer correction calculated in § 4. Note that, if one multiplies (3.18) by a, then, according to (4.20), the right-hand side is a function of a/ν only. For any value of a/ν we can thus compute a and then divide the two to get the corresponding ν. The value of a is then a good approximation to the QL value provided that ν is small enough.

In order to get a complete picture of the change in a as ν is decreased, we also carried out the linear stability analysis of the laminar solution and the weakly nonlinear analysis close to the onset of bifurcation where the condensate appears. These were performed on the QL system of equations and are described in appendix C. Although the amplitude of the condensate is small in the range of validity of the weakly nonlinear regime, results from this analysis of the QL equations agree very well with the NL solution and with the results in Thess (1992).

The amplitude a of the condensate is plotted as a function of ν^{-1} in figure 6, together with the different approximate solutions presented so far. The behaviour is qualitatively the same for $n = 2$ and $n = 6$: at high values of ν, the laminar solution in (2.2) is stable and there is no large-scale flow. The condensate appears through a supercritical bifurcation above a critical value of ν^{-1}. Close to onset, the bifurcation curve is very well captured by the weakly nonlinear analysis of the QL system in appendix C. The QL and NL values of a are monotonically increasing functions of ν^{-1}, which eventually saturate at very small viscosity. The asymptotic value of a for the QL system is given by (3.19) and (3.20), and the approach to this value as ν decreases closely follows the curve predicted by the boundary-layer analysis. This curve is fairly close to the NL curve for $n = 2$, and the QL approximation allows us to compute the amplitude of the large-scale flow within an error of only 7 % whatever the value of viscosity. Unfortunately, the error in the QL a increases to 30 % for $n = 6$. Note that for $n = 6$ the stationary condensate solution of the Navier–Stokes equation is unstable when ν^{-1} is greater than a critical value. Since the solution becomes time-dependent above this value, we followed the unstable fixed point to demonstrate saturation of the amplitude of the condensate.

5.1. *Transition to time-dependent regime*

For $n = 2$, the condensate solution is a stable fixed point at all the values of ν we examined: with $n = 2$ all the nonlinear numerical solutions presented in figure 6 are stable and steady. The situation is different for $n = 6$: the fixed point loses stability through a Hopf bifurcation above a critical value of ν^{-1}, which is between 1000 and 2000. Time series of the amplitude a of the condensate are displayed in figure 7 for small values of viscosity. When $\nu^{-1} = 1000$ the amplitude relaxes from the initial condition to the fixed point corresponding to the condensate. This fixed point is stable and the solution becomes time-independent at large time. However, for $\nu^{-1} = 2000$ the fixed point is slightly unstable. The amplitude a oscillates periodically, as can be seen in the inset of figure 7. The oscillation is very weak, a having a mean value around 0.465 and a standard deviation smaller than 10^{-5}. The system thus remains close to the fixed point. As we move to smaller values of ν, this periodic behaviour

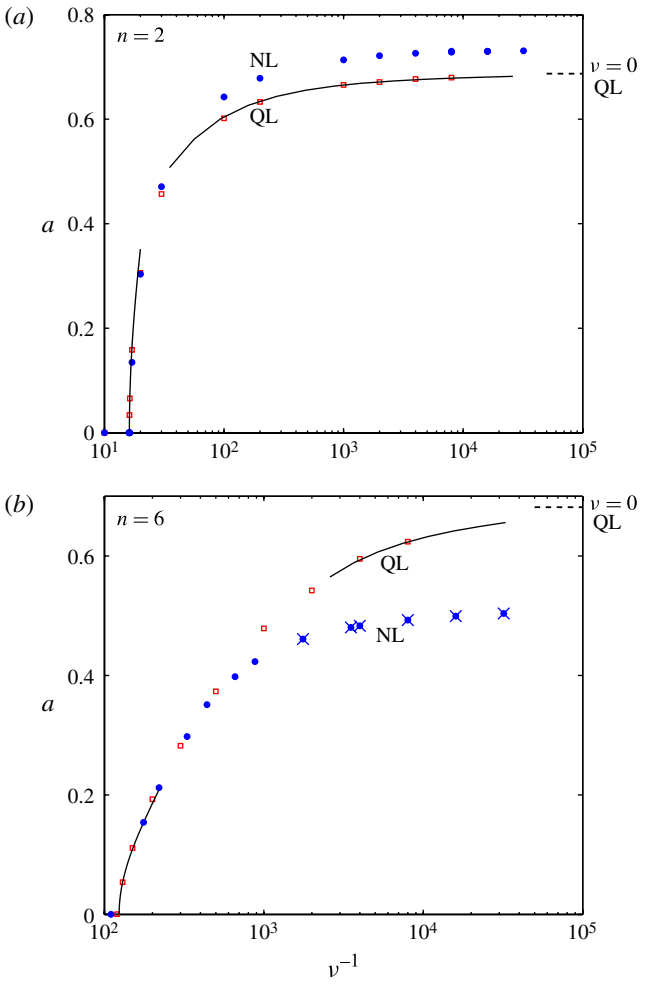

FIGURE 6. (Colour online) Amplitude of the condensate as a function of inverse viscosity (●, simulations of the NL system; □, simulations of the QL system): (*a*) $n = 2$; (*b*) $n = 6$. The solid line close to onset is the result of the weakly nonlinear analysis. The solid line at low viscosity corresponds to the boundary-layer approximation from § 4. The dashed line on the far right corresponds to the $\nu \to 0$, QL predictions in (3.19) and (3.20). In panel (*b*) the crossed symbols correspond to unstable fixed points that we followed to demonstrate saturation of the amplitude.

becomes quasi-periodic, until the system switches to the bursting behaviour illustrated in figure 7(*c*) for $\nu^{-1} = 4000$: the amplitude relaxes until it gets very close to the fixed point. However, this fixed point is slightly unstable and a 'turbulent' burst occurs. The burst is characterized by a very rapid increase in the amplitude a and a disorganized vorticity field. Close to the maximum value of a, the system settles back onto the family of inviscid solutions to the problem: vorticity becomes organized again, with a structure similar to figure 2, but with an amplitude of the condensate much larger than what viscosity would select. Subsequently $a(t)$ relaxes back towards the fixed point until another burst occurs. Similar bursting behaviour was reported in several nonlinear

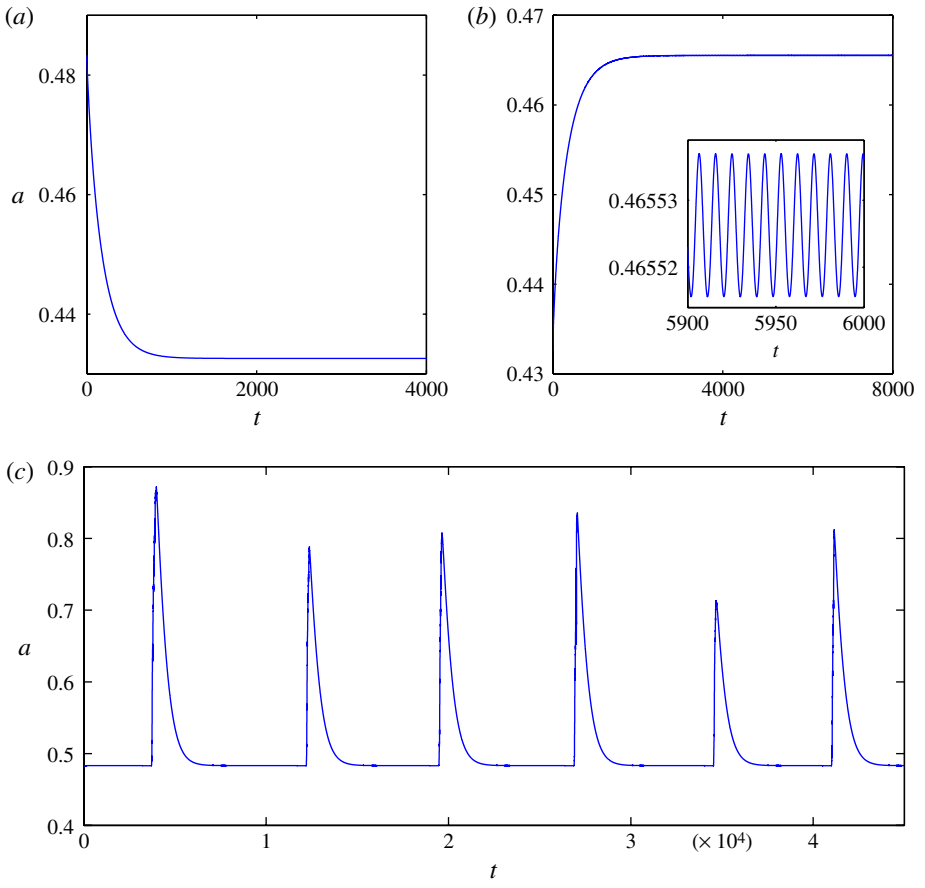

FIGURE 7. (Colour online) Amplitude of the condensate as a function of time. (*a*) At $\nu^{-1} = 1000$ the system relaxes to a steady solution. (*b*) With $\nu^{-1} = 2000$ there is weak time dependence; the inset is an expanded view showing the small oscillations in $a(t)$. (*c*) With $\nu^{-1} = 4000$ there is bursting; the system goes very close to the unstable fixed point between bursts.

dynamical systems with triadic interactions, for instance in the framework of thermal convection (Hughes & Proctor 1990; Kumar, Pal & Fauve 2006).

One way of obtaining information on a dynamical system consists in computing its unstable periodic orbits. Statistical properties of the system can then be obtained through weighted averages on these periodic orbits (Cvitanović 1988). This strategy has been applied recently to two-dimensional body-forced turbulence, considered as a dynamical system with very many degrees of freedom (Chandler & Kerswell 2012). While this approach is still limited by computational power, it could be efficient to describe the chaotic dynamical regime illustrated in figure 7, which shares common features with low-dimensional chaos.

In an unsteady situation, such as the one shown in figure 7(*c*), the theory from §§ 3 and 4 describes the amplitude of the unstable fixed point. To determine this amplitude numerically, we discovered that computations started with energy only in the gravest Fourier mode quickly converged to the unstable fixed point.

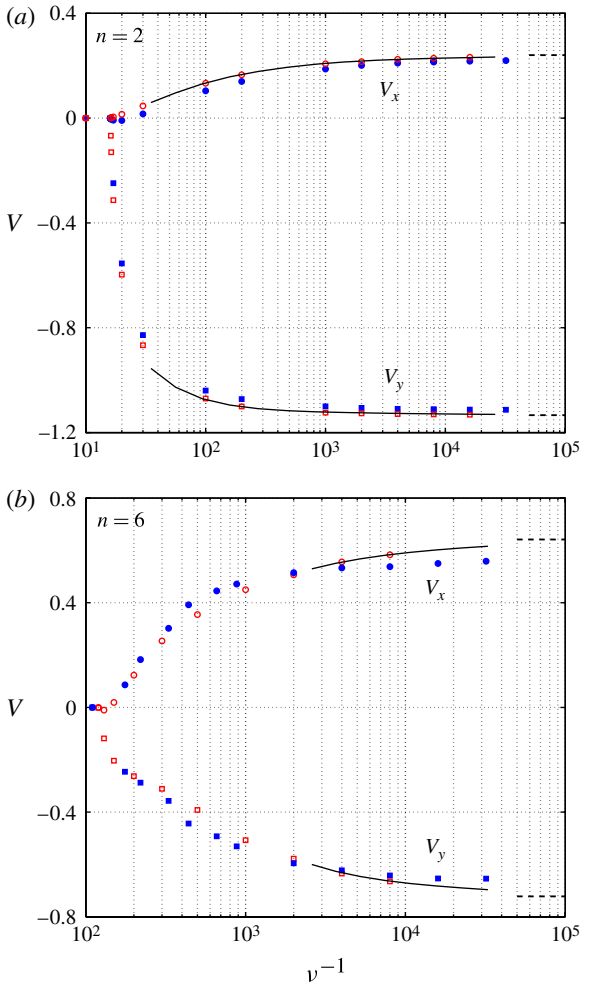

FIGURE 8. (Colour online) Boundary velocities as a function of inverse viscosity (●, V_x; □, V_y), for the same numerical simulations as in figure 6: (*a*) $n = 2$; (*b*) $n = 6$. Filled symbols are results from simulations of the NL system of equations, whereas empty symbols are results from simulations of the QL system. The solid lines correspond to the theoretical predictions from the boundary-layer approximation. The dashed lines on the far right correspond to the QL predictions in the $\nu \to 0$ limit. See figure 6 for the stability of the corresponding fixed points.

5.2. *Velocity of the large-scale circulation*

The 30 % error in the QL estimate of a for $n = 6$ comes from the fact that a is a global quantity that is sensitive to the central region of the square domain, where the velocity associated with χ vanishes. The quasilinear approximation is justified only where the large-scale flow dominates, and we expect it to give reliable predictions for the large-scale velocity field only where this velocity is large. To illustrate this matter, we now focus on the velocity of the large-scale circulation, which we evaluate as $V_x = \psi_y|_{(x=\pi/2,y=0)}$ and $V_y = -\psi_x|_{(x=0,y=\pi/2)}$. These quantities are the tangential velocities measured, respectively, at the middle of the $y = 0$ and of the $x = 0$ walls. We show them in figure 8 as functions of inverse viscosity. As expected, the agreement

is good in these peripheral regions, the error being around a few per cent for $n = 2$ and around 10 % for $n = 6$. The boundary-layer analysis provides reliable predictions of the velocities V_x and V_y at small viscosity. As ν goes to zero, these velocities saturate to asymptotic values, which can be computed in the QL approximation using the inviscid solution for ϕ. This is done numerically for $n = 6$ and analytically in appendix A for $n = 2$.

6. Triadic selection mechanism

The previous results show that the velocity of this forced two-dimensional condensate has a finite limit as $\nu \to 0$. One might say that the velocity follows a high-Reynolds-number or 'turbulent' scaling law, in contrast with the velocity field being proportional to ν^{-1} in the viscous laminar regime of (2.2). However, the condensate remains organized and steady at small viscosity, hence our description of it as a laminar condensate. Let us investigate further how this ν-independent scaling arises in the equations.

In the framework of the quasilinear approximation, we described the low-viscosity solution as the selection by the viscous term of one solution from a continuous family of solutions to the Euler equation. Similar selection mechanisms occur in soliton equations with weak forcing and dissipation (Fauve & Thual 1990; Hakim, Jakobsen & Pomeau 1990): dissipation selects the size of a soliton inside a continuous family of soliton solutions to the non-dissipative equation. However, there is one major difference between these studies and the present problem: the size of the selected soliton then depends explicitly on the relative amplitudes of the forcing and dissipative coefficients, whereas here the selected velocity field becomes independent of viscosity as $\nu \to 0$.

6.1. *A generic selection mechanism for forced triadic systems*

We now wish to generalize the selection criterion (3.17) to forcing functions that are not necessarily harmonic. Let us consider the two following transformations: $\mathscr{S}$ is the reflection with respect to $y = \pi/2$, and $\mathscr{R}$ is the rotation of angle $\pi/2$ around the centre of the square domain. We decompose the QL streamfunction into three components:

(i) $a\chi$ is the large-scale condensate, which does not change sign under $\mathscr{R}$ or $\mathscr{S}$;
(ii) $\phi^{(-1)}$ is the part of the remainder that changes sign under $\mathscr{R}$ and $\mathscr{S}$; and
(iii) $\phi^{(1)}$ is the part of the remainder that changes sign under $\mathscr{R}$ but is invariant under $\mathscr{S}$.

Figure 9 illustrates the symmetries of these three components and of the forcing function. For two components g and h of the streamfunction, one can prove the following relations for the symmetries of a nonlinear term:

$$\mathscr{R}(J(g,h)) = J(\mathscr{R}(g), \mathscr{R}(h)), \tag{6.1}$$

$$\mathscr{S}(J(g,h)) = -J(\mathscr{S}(g), \mathscr{S}(h)). \tag{6.2}$$

Using these symmetries, the QL system of equations becomes

$$(\Delta\phi^{(-1)})_t = -J(\Delta\phi^{(1)} + 2\phi^{(1)}, a\chi) + \sin nx \sin ny + \nu\Delta^2\phi^{(-1)}, \tag{6.3}$$

$$(\Delta\phi^{(1)})_t = -J(\Delta\phi^{(-1)} + 2\phi^{(-1)}, a\chi) + \nu\Delta^2\phi^{(1)} \tag{6.4}$$

$$a_t = 2\langle (J(\Delta\phi^{(-1)}, \phi^{(1)}) + J(\Delta\phi^{(1)}, \phi^{(-1)}))\chi \rangle - 2\nu a. \tag{6.5}$$

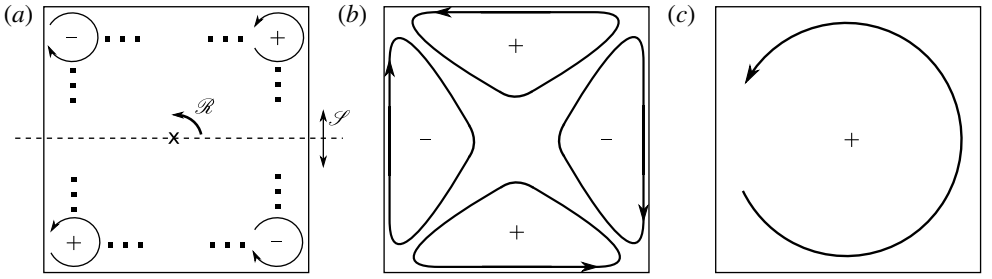

FIGURE 9. Sketch of the symmetries of the different components of the streamfunction: $\mathscr{S}$ is reflection with respect to $y = \pi/2$; $\mathscr{R}$ is rotation by angle $\pi/2$ around the centre of the square domain. (*a*) The forcing term, together with component $\phi^{(-1)}$ of the remainder, changes sign under these two transformations. (*b*) The inviscid solution for the remainder or component $\phi^{(1)}$ changes sign under $\mathscr{R}$ but not under $\mathscr{S}$. (*c*) The large-scale condensate $a\chi$ does not change sign under $\mathscr{R}$ nor $\mathscr{S}$.

Let us consider the limit of small viscosity $\nu \ll 1$ and expand $\phi^{(1)}$ and $\phi^{(-1)}$ following (3.7). To order $O(1)$, a solution is given by

$$\phi_0^{(-1)} = 0, \quad a \neq 0 \quad \text{and} \quad J(\Delta\phi_0^{(1)} + 2\phi_0^{(1)}, a\chi) = \sin nx \sin ny. \tag{6.6}$$

This corresponds to the continuous family of inviscid solutions, with $\phi_0^{(1)} \sim 1/a$. The component $\phi^{(-1)}$ comes into play at order $O(\nu)$. Equation (6.4) to order $O(\nu)$ yields

$$J(\Delta\phi_1^{(-1)} + 2\phi_1^{(-1)}, a\chi) = \Delta^2\phi_0^{(1)}. \tag{6.7}$$

The interplay between the components $\phi^{(-1)}$ and $\phi^{(1)}$ then forces the condensate, as follows from (6.5) to order $O(\nu)$:

$$\langle [J(\Delta\phi_1^{(-1)}, \phi_0^{(1)}) + J(\Delta\phi_0^{(1)}, \phi_1^{(-1)})]\chi \rangle = a. \tag{6.8}$$

Both sides of the equation are independent of ν, and a ν-independent amplitude is selected by viscosity. In contrast with (3.17), the alternate selection criterion (6.8) does not require a harmonic forcing, but it does require a small enough viscosity. These two criteria are equivalent for harmonic forcing and small enough viscosity.

Equations (6.3)–(6.5) highlight the fact that this selection mechanism occurs in a triadic system of equations. It is indeed a generic selection mechanism for a triad whose unstable degree of freedom is forced. The simplest example of such a system may be a solid, for which rotation about the axis with intermediate moment of inertia is unstable. We thus consider a solid that has angular velocities of rotation $[\Omega_1, \Omega_2, \Omega_3]$ around its principal axes of rotation, with moments of inertia, respectively, $I_1 < I_2 < I_3$. We assume that a constant torque drives the spin around the axis of intermediate moment of inertia I_2. An appropriate scaling of time, and of the three components of the rotation vector, allows us to set this torque to unity and the nonlinear coefficients to ± 1, so that the motion of the solid follows

$$\dot{\Omega}_1 = -\Omega_2\Omega_3 - \alpha\nu\Omega_1, \tag{6.9}$$

$$\dot{\Omega}_2 = 1 + \Omega_1\Omega_3 - \nu\Omega_2, \tag{6.10}$$

$$\dot{\Omega}_3 = -\Omega_1\Omega_2 - \beta\nu\Omega_3. \tag{6.11}$$

We assumed a fluid friction term in each equation, proportional to some coefficient ν. When ν is large, the solution to this system is $\Omega_1 = \Omega_3 = 0$ and $\Omega_2 = 1/\nu$: the

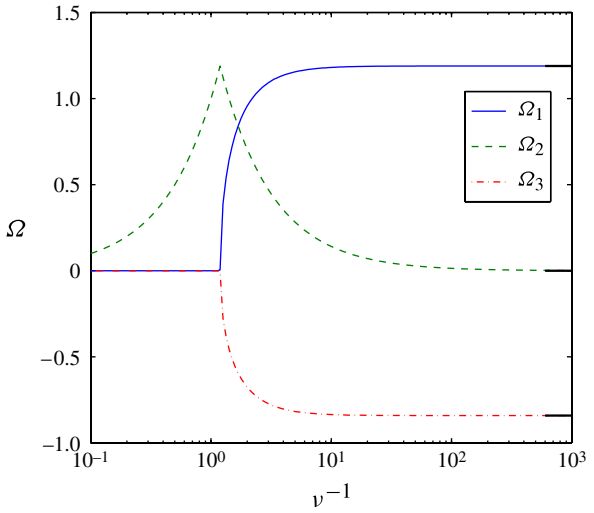

FIGURE 10. (Colour online) Steady-state solution of the system of equations (6.9)–(6.11) as a function of ν^{-1}, for $\alpha = 1$ and $\beta = 2$. The thick black lines on the right-hand side correspond to the solution (6.12), which is selected inside the continuous family of non-dissipative solutions.

solid spins around the axis of the applied torque. This is the equivalent of the viscous laminar solution to the fluid problem, where the viscous term balances the forcing. When ν decreases, this solution becomes unstable, so that Ω_1 and Ω_3 spontaneously become non-zero.

Let us now consider the non-dissipative problem, which is obtained by setting ν to zero. A solution is then $[\Omega_1, \Omega_2, \Omega_3] = [\Omega_1, 0, -1/\Omega_1]$, where at this stage any value of Ω_1 is acceptable. This is the equivalent of the continuous family of solutions to the inviscid fluid problem, with a condensate amplitude a and a remainder proportional to $1/a$. A small value of ν can then be taken into account perturbatively: Ω_2 is eliminated from the stationary versions of (6.9) and (6.11), and Ω_3 is replaced by its expression in terms of Ω_1 computed for $\nu = 0$, to give

$$\Omega_1 = \pm\left(\frac{\beta}{\alpha}\right)^{1/4}. \tag{6.12}$$

The small dissipative term selects one solution out of the continuous family of solutions, and this solution is independent of ν. We show in figure 10 how the steady state of the system of equations (6.9)–(6.11) evolves from the 'laminar' solution $\Omega_2 = 1/\nu$ to the ν-independent solution as ν decreases.

One may argue that many physical systems saturate to a solution independent of the damping coefficient as the latter goes to zero. Consider, for instance, a damped harmonic oscillator that is forced sinusoidally away from resonance: as the dissipation coefficient goes to zero, the amplitude of oscillation saturates to a finite value, independent of the small damping coefficient. There is, however, one major difference between such systems and the triadic systems we are dealing with in this study: the damped harmonic oscillator has only one asymptotic amplitude when dissipation is set to zero. No matter the structure of the dissipative term of the equation (it can be proportional to velocity, to some higher-order time derivative of position, or it can

even be nonlinear), the system will eventually saturate to this asymptotic amplitude, computed for the non-damped problem, as the damping coefficient goes to zero. But in triadic systems one cannot predict the asymptotic solution by studying only the non-damped problem: there is a continuous family of solutions, and the selected solution strongly depends on the structure of the dissipative terms of the equations. An illustration of this phenomenon is given by (6.12), where the selected amplitude depends on α and β. A different structure of the dissipative term, given by different values of α and β, will select another solution out of the continuous family of solutions to the non-damped problem.

7. Dependence of the condensate on the form of dissipation

To show that the triadic mechanism described in § 6 operates in the nonlinear Navier–Stokes equation, as well as in the QL approximation, we demonstrate in this section that the amplitude of the condensate depends on the form of the dissipation.

7.1. *Bottom drag*

We first consider a combination of viscosity and bottom drag:

$$\Delta\psi_t + J(\Delta\psi, \psi) = \sin nx \sin ny + \nu\Delta^2\psi - \nu\gamma\Delta\psi. \tag{7.1}$$

The drag coefficient is denoted as $\nu\gamma$, where $\gamma = 0$ corresponds to the Navier–Stokes equation without drag, and increasing γ allows us to modify the structure of the dissipative term continuously. Although the physically relevant regime is $\gamma \geqslant 0$, we can consider negative values of γ provided $\gamma > -2$. This condition ensures that the dissipative term of (7.1) linearly damps every Fourier mode of the square domain.

We are interested in the solution of this equation as ν goes to zero. We thus followed the fixed point obtained for $\gamma = 0$ into the $\gamma \neq 0$ regime, and we plot in figure 11 the amplitudes of the condensate and boundary velocities as a function of γ for several (small) values of ν. We observe that:

(i) the amplitude is almost independent of ν for these small values of ν; and

(ii) the amplitude strongly depends on γ, and thus on the structure of the dissipative term.

In the framework of the quasilinear approximation, we can compute the dependence of the amplitude a of the condensate as a function of γ, for $\nu \to 0$. We include bottom drag in the QL system of equations before computing the energy and enstrophy budgets to get the equivalents of (3.15) and (3.16). Eliminating injection of energy and enstrophy from the forcing leads to the following expression for the amplitude of the condensate:

$$a = \pm\sqrt{\frac{\langle|\nabla\Delta\phi|^2\rangle - 2n^2\gamma\langle|\nabla\phi|^2\rangle + (\gamma - 2n^2)\langle(\Delta\phi)^2\rangle}{(2+\gamma)(n^2-1)}}, \tag{7.2}$$

where ϕ can be replaced by the inviscid solution for the remainder, ϕ_0. For a given n, this expression for a only depends on γ and thus on the structure, but not the strength, of the dissipative term. For $n = 2$ the spatial averages are computed in appendix A, which yields

$$|a(\gamma)| = \left[\frac{(795 - 70\pi^2 - \pi^4)\gamma + (750 - 40\pi^2 - 2\pi^4)}{360(\gamma + 2)}\right]^{1/4}. \tag{7.3}$$

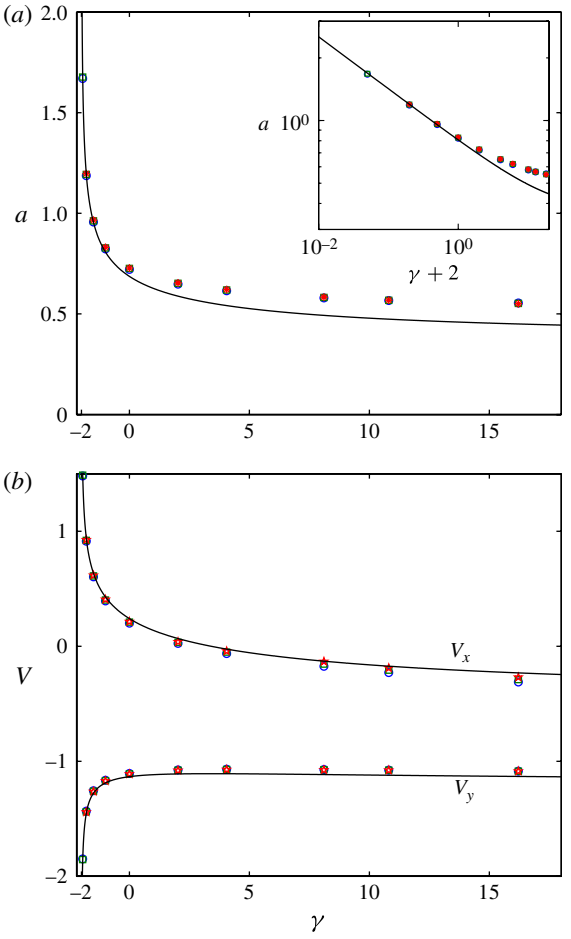

FIGURE 11. (Colour online) Dependence of the condensate's amplitude and boundary velocities on the ratio γ of bottom drag to viscosity, for $n = 2$ forcing. The curve is rather independent of ν^{-1} for these low values of ν and the selected solution depends only on the structure of the dissipative term (●, $\nu^{-1} = 2000$; □, $\nu^{-1} = 4000$; ⋆, $\nu^{-1} = 8000$; solid lines, predictions from QL theory). Numerical points computed for strictly positive γ are unstable fixed points (see text). (*a*) Amplitude of the condensate. The inset is a log–log representation of this amplitude as a function of $\gamma + 2$, to demonstrate the asymptotic validity of the QL theory. (*b*) Boundary velocities.

The boundary velocities are then given by $V_x = (\ln 2 - 1)/a(\gamma) + a(\gamma)$ and $V_y = (\ln 2 - 1)/a(\gamma) - a(\gamma)$. These predictions are compared to the numerical results in figure 11. As expected, the agreement between the NL simulations and the QL predictions is better for the boundary velocities than for the amplitude of the condensate. The amplitude $a(\gamma)$ diverges in the limit $\gamma \to -2$, for which the total linear damping on the gravest mode vanishes in (7.1). The condensate then strongly dominates the remainder, meaning that the quasilinear approximation is asymptotically exact in the limit $\gamma \to -2$. Indeed, the QL solution captures exactly the asymptotic behaviour of the full nonlinear system in this limit, as can be seen in the inset of figure 11. It provides fairly accurate estimates for the boundary velocities all the way to the physically relevant domain of positive γ.

We stress that even a slight (positive) bottom drag can make the fixed point unstable, so that the solution becomes time-dependent. Time dependence induced by drag can be more dramatic than the bursting shown in figure 7: with large enough drag the sign of the vortex condensate episodically reverses (Sommeria 1986; Gallet *et al.* 2011). We then followed the fixed point, starting the simulations with energy in the gravest mode only. The results in figure 11 should thus be considered more as a proof that the amplitude of the condensate depends on the structure of the dissipative term, than as predictions of the behaviour of two-dimensional flows with bottom-drag damping.

7.2. *Hyperviscosity*

A common approximation in numerical simulations consists in replacing the usual viscous term of the Navier–Stokes equation (2.1) by a hyperviscosity, $\nu_p \Delta^{2p} \psi$. The Navier–Stokes case is $p = 1$, but larger values of p are often used. This seems rather harmless when viscosity is only expected to remove energy and enstrophy in the high-wavenumber modes, at the end of a forward turbulent cascade. However, in the present study there is no such cascade. Indeed, the nonlinear interaction is non-local in Fourier space, between a condensate with wavenumber $O(1)$ and a smaller-scale remainder with wavenumber $O(n)$. Although the flow becomes independent of viscosity when $\nu \to 0$, we stress the fact that the flow depends strongly on the structure of the dissipative term. Therefore, we expect that replacing the viscous term by a hyperviscosity might modify the amplitude of the condensate. Indeed, with a hyperviscous term $\nu_p \Delta^{2p} \psi$, (3.18) for the condensate amplitude becomes

$$a = \pm \sqrt{\frac{\langle |\boldsymbol{\nabla} \Delta^p \phi|^2 \rangle - 2n^2 \langle (\Delta^p \phi)^2 \rangle}{2^{2p-1}(n^2 - 1)}}, \tag{7.4}$$

which we consider for $p \geqslant 2$. The situation is then problematic in the limit $\nu_p \to 0$, since the integrals corresponding to the spatial averages on the right-hand side of (7.4) do not converge if ϕ is replaced by the inviscid solution ϕ_0: hyperviscous boundary layers must always be included in the expression for ϕ, and the amplitude a always depends explicitly on ν_p. If $p \geqslant 2$ then the amplitude of the condensate tends to infinity as $\nu_p \to 0$. To summarize, our conclusion that the amplitude of the condensate is independent of viscosity as $\nu \to 0$ depends crucially on the dissipative term being of standard Navier–Stokes type with $p = 1$. Hyperviscosity entails an unfortunate dependence of condensate amplitude on the magnitude of the unphysical parameter ν_p.

8. Conclusion

Direct numerical solutions of the two-dimensional Navier–Stokes equation, driven by steady forcing applied to a single mode, show the formation of a steady vortex condensate. The streamfunction of the condensate projects strongly onto the gravest mode of the square container, and this observation motivates the development of a quasilinear approximation that roughly determines the amplitude of the condensate. Although the viscous term of the Navier–Stokes equation is crucial in selecting the amplitude from a continuous family of solutions to the forced Euler equation, the selected solution is independent of ν as $\nu \to 0$.

A common belief in forced two-dimensional turbulence is that energy accumulates in the gravest mode until either the numerical simulation diverges, or the large-scale velocity reaches extremely large values (infinitely large as viscosity goes to zero). This is indeed the case for flows driven by white-noise-in-time forcing. Such forcing

injects energy at a constant rate, ε in (3.14), and this energy eventually accumulates in a large-scale condensate. The system saturates when viscous dissipation acting on the large-scale velocity balances energy injection, resulting in a typical velocity proportional to $(\varepsilon/\nu)^{1/2}$. By contrast, this study shows that, for a steady forcing, energy injection switches off when the large-scale flow is vigorous enough, so that the large-scale vortex saturates to a ν-independent value. The mechanism by which this saturation occurs is described in Tsang & Young (2009): at small viscosity, advection of forcing-scale eddies by the large-scale vortex breaks the phase relation between these structures and the forcing, and so limits energy injection. In the present study, with steady Kolmogorov forcing, we have shown that energy injection ε is proportional to ν as $\nu \to 0$. This scaling is consistent with the rigorous bounds on ε derived by Alexakis & Doering (2006), who showed that ε goes to zero proportionally to ν as $\nu \to 0$ for constant root-mean-square velocity. However, the scaling in this paper is a significantly stronger result: energy injection goes to zero proportionally to ν for *constant forcing amplitude*. This is a key difference between the time-independent forcing protocols most often used in experiments and the white-noise forcing used in many numerical simulations.

These conclusions challenge the applicability of statistical theories of the two-dimensional Euler equation to real two-dimensional flows with weak injection and dissipation of energy. Indeed, the rationale behind these theories is that the vanishingly small injection and dissipation of energy can be largely ignored in computing the final state of the flow using statistical mechanics. Our analytical and numerical computations show that, although energy dissipation is small for small damping coefficient, the final state of the flow strongly depends on the 'form' of the damping (whether it is usual viscosity, bottom drag, or a combination of both), regardless of how small the damping coefficients and energy dissipation are. Indeed, the dependence of the amplitude of the large-scale vortex with the form of the dissipative term, represented in figure 11, cannot be captured by a theory that neglects all dissipative terms at the outset. It remains to be investigated whether the triadic selection mechanism described in this paper could select one solution out of a family of solutions computed using statistical mechanics of the Euler equation, thus reconciling the two approaches.

Acknowledgements

We thank S. Fauve, F. Pétrélis and Y.-K. Tsang for insightful discussions. This research was supported by the National Science Foundation under OCE07-26320. B.G. was partially supported by a Scripps Postdoctoral Fellowship.

Appendix A. Analytic expression of the QL streamfunction for $n = 2$

Starting with the $n = 2$ inviscid solution in (3.11), we need to solve the forced Helmholtz equation:

$$\Delta(a\phi_0) + 2(a\phi_0) = 2\sin x \sin y \ln(\sin x) - 2\sin x \sin y \ln(\sin y). \tag{A 1}$$

The structure of the right-hand side suggests looking for a solution $a\phi_0 = P(x)\sin y - P(y)\sin x$. Substitution into (A 1) yields

$$P''(x) + P(x) = 2\sin(x)\ln(\sin x) + C\sin x, \tag{A 2}$$

where C is a separation constant. The last term, $C\sin x$, does not contribute to the left-hand side of (A 1). It is however necessary to fulfil the solvability condition

imposed by multiplying (A 2) by $\sin x$ and integrating from 0 to π: C must be chosen to cancel out with the first term in the Fourier series of $2\sin(x)\ln(\sin x)$, so that the right-hand side of the equation has no resonant term. This Fourier series is

$$2\sin(x)\ln(\sin x) = \frac{1-2\ln 2}{2}\sin x - \sum_{p=1}^{\infty}\frac{\sin((2p+1)x)}{p(p+1)}. \tag{A 3}$$

Hence $C = (2\ln 2 - 1)/2$ and

$$P(x) = \sum_{p=1}^{\infty}\frac{\sin((2p+1)x)}{4p^2\,(p+1)^2}. \tag{A 4}$$

With the function P in hand, expressions for the remainder $a\phi_0$, its vorticity and the viscous term are then obtained as

$$a\phi_0 = \sum_{p=1}^{\infty}\frac{1}{4p^2\,(p+1)^2}[\sin y\sin((2p+1)x) - \sin x\sin((2p+1)y)], \tag{A 5}$$

$$\Delta(a\phi_0) = -\sum_{p=1}^{\infty}\frac{(2p+1)^2+1}{4p^2\,(p+1)^2}[\sin y\sin((2p+1)x) - \sin x\sin((2p+1)y)], \tag{A 6}$$

$$\Delta^2(a\phi_0) = \sum_{p=1}^{\infty}\frac{((2p+1)^2+1)^2}{4p^2\,(p+1)^2}[\sin y\sin((2p+1)x) - \sin x\sin((2p+1)y)]. \tag{A 7}$$

The averages involved in the determination of a can now be evaluated:

$$\langle a\phi_0\Delta(a\phi_0)\rangle = -\frac{1}{32}\sum_{p=1}^{\infty}\frac{1+(2p+1)^2}{p^4\,(p+1)^4} = \frac{675-60\pi^2-\pi^4}{720}, \tag{A 8}$$

$$\langle[\Delta(a\phi_0)]^2\rangle = \frac{1}{2}\sum_{p=1}^{\infty}\left[\frac{1+(2p+1)^2}{4p^2\,(p+1)^2}\right]^2 = \frac{-315+30\pi^2+\pi^4}{360}, \tag{A 9}$$

$$\langle\Delta^2(a\phi_0)\Delta(a\phi_0)\rangle = -\frac{1}{32}\sum_{p=1}^{\infty}\frac{[1+(2p+1)^2]^3}{p^4\,(p+1)^4} = \frac{135-60\pi^2-\pi^4}{180}. \tag{A 10}$$

Substitution into (3.18) gives the asymptotic amplitude of the condensate as ν goes to zero:

$$|a| = \frac{\left(75-4\pi^2-\dfrac{\pi^4}{5}\right)^{1/4}}{2^{3/4}\sqrt{3}} \simeq 0.687. \tag{A 11}$$

The boundary velocities $V_x = a + \phi_y|_{(x=\pi/2,y=0)}$ and $V_y = -a - \phi_x|_{(x=0,y=\pi/2)}$ are finally

$$V_x = a + \frac{1}{a}\sum_{p=1}^{\infty}\frac{(-1)^p-(2p+1)}{4p^2\,(p+1)^2} = a + \frac{\ln 2-1}{a} \simeq 0.2404, \tag{A 12}$$

$$V_y = -a + \frac{\ln 2-1}{a} \simeq -1.1337, \tag{A 13}$$

where the numerical values are given for positive a.

If bottom friction is included, this asymptotic amplitude is given by (7.2), which reduces to

$$|a(\gamma)| = \left[\frac{(795 - 70\pi^2 - \pi^4)\gamma + (750 - 40\pi^2 - 2\pi^4)}{360(\gamma + 2)}\right]^{1/4}. \tag{A 14}$$

This expression gives (A 11) for $\gamma = 0$. The boundary velocities are still given by

$$V_x = a(\gamma) + \frac{\ln 2 - 1}{a(\gamma)}, \tag{A 15}$$

$$V_y = -a(\gamma) + \frac{\ln 2 - 1}{a(\gamma)}. \tag{A 16}$$

For $n = 6$ and no bottom drag, the inversion of expression (3.12) is performed numerically in Fourier space to get the streamfunction. Then the integrals (A 9) and (A 10) are computed together with the derivative of ϕ at the middle point of a boundary. This yields the following approximate values for the solution of the quasilinear problem in the $\nu \to 0$ limit:

$$|a| \simeq 0.682, \tag{A 17}$$

$$V_x \simeq 0.642, \tag{A 18}$$

$$V_y \simeq -0.722, \tag{A 19}$$

where the numerical values of the velocities are given for positive a.

Appendix B. Asymptotic behaviour of the inner solution

To characterize the behaviour of s in (4.19) for small and large $\chi/\sqrt{\nu}$, we study the function

$$f(x, b) \stackrel{def}{=} \sum_{p=0}^{\infty} \frac{(-1)^p}{\sqrt{p + b}} \mathscr{D}\left(\frac{x}{\sqrt{p + b}}\right), \tag{B 1}$$

with $b > 0$. In (B 1), $\mathscr{D}$ is Dawson's integral defined in (4.18).

For small x, each term of the series (B 1) can be expanded to give

$$f(x, b) = x \sum_{p=0}^{\infty} \frac{(-1)^p}{p + b} + O(x^3). \tag{B 2}$$

For large x , the behaviour of the function in (B 1) can be computed using Mellin's transform (Davies 2000), which is defined by

$$f^*(z, b) = \int_0^{\infty} f(x, b) x^{z-1}\, \mathrm{d}x. \tag{B 3}$$

The Mellin transform factors the sum in (B 1):

$$f^*(z, b) = \mathscr{D}^*(z) \sum_{p=0}^{\infty} (-1)^p \left(\sqrt{p + b}\right)^{z-1} \tag{B 4}$$

$$= \mathscr{D}^*(z) 2^{(z-1)/2} \left[\mathscr{H}\left(\frac{1 - z}{2}, \frac{b}{2}\right) - \mathscr{H}\left(\frac{1 - z}{2}, \frac{1 + b}{2}\right)\right], \tag{B 5}$$

where

$$\mathscr{D}^*(z) = \frac{\sqrt{\pi}}{4} \tan\left(\frac{\pi z}{2}\right) \Gamma\left(\frac{z}{2}\right) \tag{B 6}$$

is Mellin's transform of Dawson's integral. Equation (B 5) involves the Hurwitz zeta function $\mathscr{H}$, which permits an analytic continuation of the infinite sum to $z \geqslant 1$. Each pole of Mellin's transform corresponds to a term in the asymptotic development of the corresponding function. A simple pole on the real axis at a value z_0 corresponds to a term proportional to x^{-z_0} in the expansion of the function, the prefactor being proportional to the residue. Poles on the negative real axis therefore determine the Taylor expansion of the function around $x = 0$ in powers of x, whereas poles on the positive real axis determine its asymptotic expansion for large x in terms of inverse powers of x.

Dawson's integral $\mathscr{D}(x)$ admits a regular asymptotic expansion at infinity in terms of odd powers of $1/x$, the first and dominant term being $1/(2x)$. Its Mellin transform therefore has poles at each odd positive integer. The essential property of the Hurwitz zeta function that we invoke is that the bracketed term in (B 5) has no poles in the complex plane, so that f^* has the same poles as $\mathscr{D}^*$. Hence $f(x)$ behaves as $1/x$ for large x, the prefactor being the $1/x$ coefficient of $\mathscr{D}$ multiplied by the bracketed term evaluated at $z = 1$. The behaviour of $f(x, b)$ at large x is finally

$$f(x, b) = \frac{1}{2x}\left[\mathscr{H}\left(0, \frac{b}{2}\right) - \mathscr{H}\left(0, \frac{1+b}{2}\right)\right] + O(1/x^3) = \frac{1}{4x} + O(1/x^3). \tag{B 7}$$

The behaviour of s for large χ is then computed using

$$s(\tau, \chi) = -\frac{4}{\sqrt{2a\nu}} f\left(\frac{\chi}{2}\sqrt{\frac{a}{2\nu}}, \frac{\tau}{2}\right) \sim -\frac{2}{a\chi}, \tag{B 8}$$

so that the inner solution (4.20) away from the boundary layers is approximately

$$\Delta q^{(i)} \simeq \frac{2}{a}\left(\frac{\sin y}{\sin x} - \frac{\sin x}{\sin y}\right). \tag{B 9}$$

This matches the dominant behaviour of the outer solution – the Laplacian of (3.11) – close to the boundaries.

Appendix C. Weakly nonlinear analysis around the viscous laminar solution

When viscosity decreases, the viscous laminar solution (2.2) becomes unstable and a large-scale condensate appears. A linear stability analysis allows one to compute the threshold of instability, and a weakly nonlinear expansion gives access to the amplitude of the condensate as a function of the departure from onset. For simplicity, we perform these analyses on the QL system of equations (3.4) and (3.5). We are looking for stationary bifurcations to stationary solutions of the system, so we discard time derivatives in these equations. The laminar solution of the system is $\psi_L = -\sin nx \sin ny/(4\nu n^4)$, and ψ_L becomes unstable when the viscosity is below a critical value ν_c. Let us consider a small parameter $\epsilon \ll 1$ and introduce the scalings

$$\nu = \nu_c - \epsilon^2\delta, \tag{C 1}$$

$$a = \epsilon a^{(0)} + \epsilon^2 a^{(1)} + \epsilon^3 a^{(2)} + \cdots, \tag{C 2}$$

$$\phi = \psi_L + \epsilon\phi^{(0)} + \epsilon^2\phi^{(1)} + \epsilon^3\phi^{(2)} + \cdots, \tag{C 3}$$

where ν_c is still to be determined. At order ϵ^0, the forcing is balanced by the viscous term from the laminar solution. At order ϵ^1, (3.4) gives the spatial structure of the eigenmode for the remainder

$$\nu_c \Delta^2 \phi^{(0)} = a^{(0)} J(\Delta\psi_L + 2\psi_L, \chi) = \frac{a^{(0)}(n^2-1)}{2n^4\nu_c} J(\sin nx \sin ny, \chi), \tag{C 4}$$

where

$$J(\sin nx \sin ny, \chi) = \frac{n}{2}[\sin((n+1)x)\sin((n-1)y) - \sin((n-1)x)\sin((n+1)y)] \tag{C 5}$$

and $\Delta(J(\sin nx \sin ny, \chi)) = -2(n^2+1)J(\sin nx \sin ny, \chi)$. The Laplacian applied to $\phi^{(0)}$ is therefore simply a multiplication by $-2(n^2+1)$. In the following we write $\phi^{(0)} = a^{(0)}\mathscr{P}_0$, where

$$\mathscr{P}_0 = \frac{n^2-1}{8n^4(n^2+1)^2\nu_c^2} J(\sin nx \sin ny, \chi). \tag{C 6}$$

Equation (3.5) at order ϵ^1 is

$$\langle J(\Delta\psi_L, \phi^{(0)}) + J(\Delta\phi^{(0)}, \psi_L)\rangle = \nu_c a^{(0)}, \tag{C 7}$$

which reduces to

$$\nu_c a^{(0)} = -2\langle J(\psi_L, \chi)\phi^{(0)}\rangle = \frac{\nu_c}{a^{(0)}(n^2-1)}\langle(\Delta\phi^{(0)})^2\rangle = a^{(0)}\frac{(n^2-1)}{128\nu_c^3(n^2+1)^2n^6}. \tag{C 8}$$

Asking for a non-trivial solution $a^{(0)} \neq 0$ yields the critical value of viscosity

$$\nu_c = \left[\frac{n^2-1}{128n^6(n^2+1)^2}\right]^{1/4}, \tag{C 9}$$

under which the viscous laminar solution is unstable.

At order ϵ^2 (3.4) becomes

$$\nu_c \Delta^2 \phi^{(1)} = \delta\Delta^2\psi_L + a^{(1)} J(\Delta\psi_L + 2\psi_L, \chi) + a^{(0)} J(\Delta\phi^{(0)} + 2\phi^{(0)}, \chi), \tag{C 10}$$

with solution

$$\phi^{(1)} = \frac{\delta}{\nu_c}\psi_L + a^{(1)}\mathscr{P}_0 + (a^{(0)})^2\mathscr{P}_1, \tag{C 11}$$

where

$$\mathscr{P}_1 = \frac{n^2-1}{4\nu_c^3(n^2+1)^2}\Delta^{-2}\{J(J(\sin nx \sin ny, \chi), \chi)\} \tag{C 12}$$

is a function of x and y only for a given n. Equation (3.5) is automatically satisfied at order ϵ^2.

Equation (3.4) gives at order ϵ^3

$$\begin{aligned}\nu_c \Delta^2 \phi^{(2)} = {} & \delta\Delta^2\phi^{(0)} + a^{(2)} J(\Delta\psi_L + 2\psi_L, \chi) + a^{(1)} J(\Delta\phi^{(0)} + 2\phi^{(0)}, \chi) \\ & + a^{(0)} J(\Delta\phi^{(1)} + 2\phi^{(1)}, \chi),\end{aligned} \tag{C 13}$$

the solution of which is

$$\phi^{(2)} = \left(a^{(2)} + \frac{2\delta a^{(0)}}{\nu_c}\right)\mathscr{P}_0 + (\text{term prop. to } \mathscr{P}_1) + (a^{(0)})^3\mathscr{P}_2, \tag{C 14}$$

where the term proportional to $\mathscr{P}_1$ has no contribution in what follows, and

$$\mathscr{P}_2 = \frac{1}{\nu_c}\Delta^{-2}\{J(\Delta\mathscr{P}_1 + 2\mathscr{P}_1, \chi)\} \tag{C 15}$$

is a function of x and y only for a given n. Equation (3.5) at order ϵ^3 finally gives the amplitude $a^{(0)}$ as a function of the distance from onset:

$$(a^{(0)})^2 = -4\delta\left[\langle\chi J(\Delta\mathscr{P}_1 + 2(n^2+1)\mathscr{P}_1, \mathscr{P}_0)\rangle + \langle\chi J(\Delta\mathscr{P}_2 + 2n^2\mathscr{P}_2, \psi_L)\rangle\right]^{-1}, \tag{C 16}$$

which we rewrite in terms of the control parameter ν^{-1} as

$$a \simeq \pm\frac{2\nu_c\sqrt{\nu^{-1} - \nu_c^{-1}}}{\sqrt{\langle\chi J(\mathscr{P}_0, \Delta\mathscr{P}_1 + 2(n^2+1)\mathscr{P}_1)\rangle + \langle\chi J(\psi_L, \Delta\mathscr{P}_2 + 2n^2\mathscr{P}_2)\rangle}}. \tag{C 17}$$

Numerical values are

$$\nu_c^{-1} = 16.164 \quad \text{and} \quad a \simeq 0.1795\sqrt{\nu^{-1} - \nu_c^{-1}} \quad \text{for } n = 2; \tag{C 18}$$

$$\nu_c^{-1} = 123.63 \quad \text{and} \quad a \simeq 0.02127\sqrt{\nu^{-1} - \nu_c^{-1}} \quad \text{for } n = 6. \tag{C 19}$$

The results of this analysis are presented in figure 6. Close to onset, the good agreement with results from the simulation of the NL system is an *a posteriori* justification for using the QL system of equations. For $n = 2$ the threshold can be compared to the linear stability analysis performed by Thess (1992) on the full Navier–Stokes equation. Using our notation, Thess's result translates into $\nu_c^{-1} = 16.43$: the QL approximation predicts the threshold with a 2 % error.

REFERENCES

ALEXAKIS, A. & DOERING, C. R. 2006 Energy and enstrophy dissipation in steady state 2D turbulence. *Phys. Lett.* A **359**, 652–657.

BOFFETTA, S. 2007 Energy and enstrophy fluxes in the double cascade of two-dimensional turbulence. *J. Fluid Mech.* **589**, 253–360.

CHANDLER, G. J. & KERSWELL, R. R. (2012) Simple invariant solutions embedded in two-dimensional Kolmogorov turbulence. *J. Fluid Mech.* (accepted).

CHERTKOV, M., CONNAUGHTON, C., KOLOKOLOV, I. & LEBEDEV, V. 2007 Dynamics of energy condensation in two-dimensional turbulence. *Phys. Rev. Lett.* **99**, 084501.

CHERTKOV, M., KOLOKOLOV, I. & LEBEDEV, V. 2010 Universal velocity profile for coherent vortices in two-dimensional turbulence. *Phys. Rev.* E **81**, 015302.

CHILDRESS, S. 1979 Alpha effect in flux ropes and sheets. *Phys. Earth Planet. Inter.* **20**, 172–180.

CVITANOVIĆ, P. 1988 Invariant measurement of strange sets in terms of cycles. *Phys. Rev. Lett.* **61**, 24.

DAVIES, B. 2000 *Integral Transforms and Their Applications*. Springer.

FAUVE, S. & THUAL, O. 1990 Solitary waves generated by subcritical instabilities in dissipative systems. *Phys. Rev. Lett.* **64**, 3.

GALLET, B., HERAULT, J., LAROCHE, C., PÉTRÉLIS, F. & FAUVE, S. 2011 Reversals of a large-scale field generated over a turbulent background. *Geophys. Astrophys. Fluid Dyn.* **106** (4–5), 468–492.

GAMA, S., VERGASSOLA, M. & FRISCH, U. 1994 Negative eddy viscosity in isotropically forced two-dimensional flow: linear and nonlinear dynamics. *J. Fluid Mech.* **260**, 95–126.

HAKIM, V., JAKOBSEN, P. & POMEAU, Y. 1990 Fronts versus solitary waves in nonequilibrium systems. *Europhys. Lett.* **11**, 1.

HUGHES, D. W. & PROCTOR, M. R. E. 1990 A low-order model of the shear instability of convection: chaos and the effect of noise. *Nonlinearity* **3**, 127–153.

KRAICHNAN, R. H. 1967 Inertial ranges in two-dimensional turbulence. *Phys. Fluids* **10**, 7.

KUMAR, K., PAL, P. & FAUVE, S. 2006 Critical bursting. *Europhys. Lett.* **74**, 6.

LILLY, D. K. 1969 Numerical simulation of two-dimensional turbulence. *Phys. Fluids* **12** (Suppl.), II-240.

MALTRUD, M. E. & VALLIS, G. K. 1991 Energy spectra and coherent structures in forced two-dimensional and beta-plane turbulence. *J. Fluid Mech.* **228**, 321–342.

MESHALKIN, L. D. & SINAI, YA. G. 1961 Investigation of the stability of a stationary solution of a system of equations for the plane movement of an incompressible viscous fluid. *J. Appl. Mech.* **25**, 1700–1705.

PARET, J., JULLIEN, M.-C. & TABELING, P. 1999 Vorticity statistics in the two-dimensional enstrophy cascade. *Phys. Rev. Lett.* **83**, 17.

PARET, J. & TABELING, P. 1997 Experimental observation of the two-dimensional inverse energy cascade. *Phys. Rev. Lett.* **79**, 21.

ROSENBLUTH, M. N., BERK, H. L., DOXAS, I. & HORTON, W. 1987 Effective diffusion in laminar convective flows. *Phys. Fluids* **30**, 2636.

RUTGERS, M. A. 1998 Forced 2D turbulence: experimental evidence of simultaneous inverse energy and forward enstrophy cascades. *Phys. Rev. Lett.* **81**, 11.

SIVASHINSKY, G. I. 1985 Weak turbulence in periodic flows. *Physica* **17D**, 243–255.

SMITH, L. & YAKHOT, V. 1994 Finite-size effects in forced two-dimensional turbulence. *J. Fluid Mech.* **274**, 115–138.

SOMMERIA, J. 1986 Experimental study of the two-dimensional inverse energy cascade in a square box. *J. Fluid Mech.* **170**, 139–168.

THESS, A. 1992 Instabilities in two-dimensional spatially periodic flows. Part II: Square eddy lattice. *Phys. Fluids* A **4**, 7.

TSANG, Y.-K. 2010 Non-universal velocity probability densities in forced two-dimensional turbulence: the effect of large-scale dissipation. *Phys. Fluids* A **22**, 115102.

TSANG, Y.-K. & YOUNG, W. R. 2009 Forced-dissipative two-dimensional turbulence: a scaling regime controlled by drag. *Phys. Rev.* E **79**, 045308.